

**Lattice stability and high-pressure melting mechanism of dense hydrogen up to 1.5 TPa**Hua Y. Geng,<sup>1,2</sup> R. Hoffmann,<sup>2</sup> and Q. Wu<sup>1</sup><sup>1</sup>*National Key Laboratory of Shock Wave and Detonation Physics, Institute of Fluid Physics, CAEP; P.O. Box 919-102 Mianyang, Sichuan, 621900, People's Republic of China*<sup>2</sup>*Department of Chemistry and Chemical Biology, Cornell University, Baker Laboratory, Ithaca, New York 14853, USA*  
(Received 11 October 2014; revised manuscript received 20 July 2015; published 2 September 2015)

Lattice stability and metastability, as well as melting, are important features of the physics and chemistry of dense hydrogen. Using *ab initio* molecular dynamics (AIMD), the classical superheating limit and melting line of metallic hydrogen are investigated up to 1.5 TPa. The computations show that the classical superheating degree is about 100 K, and the classical melting curve becomes flat at a level of 350 K when beyond 500 GPa. This information allows us to estimate the well depth and the potential barriers that must be overcome when the crystal melts. Inclusion of nuclear quantum effects (NQE) using path integral molecular dynamics (PIMD) predicts that both superheating limit and melting temperature are lowered to below room temperature, but the latter never reaches absolute zero. Detailed analysis indicates that the melting is thermally activated, rather than driven by pure zero-point motion (ZPM). This argument was further supported by extensive PIMD simulations, demonstrating the stability of *Fddd* structure against liquefaction at low temperatures.

DOI: [10.1103/PhysRevB.92.104103](https://doi.org/10.1103/PhysRevB.92.104103)

PACS number(s): 67.80.F-, 62.50.-p, 64.70.dj, 71.15.Nc

**I. INTRODUCTION**

Hydrogen, the simplest element, shows complex behavior under compression [1–6]. It has at least four allotropes in the solid state that were already known, and exhibits an anomalous melting temperature ( $T_m$ ) that peaks at about 100 GPa [7–13] and then decreases downwards [12–15]. It was speculated that at higher pressures dense hydrogen in a metallic state might melt, driven not by thermal motion of nuclei (as other elements usually are) but rather by pure nuclear quantum effects (NQE), or equivalently, by the zero-point motion (ZPM) of nuclei [16,17]. This conjecture is tantalizing and hints at the possibility of a quantum liquid in its ground state as 0 K is approached [18].

Recent numerical simulations predicted that this descent might continue beyond 1 TPa [19]. However, there are two fundamental questions yet to be answered: (i) Does dense hydrogen really melt at 0 K? (ii) What are the respective roles played by the softening of the interaction potential, as well as that played by the NQE in this decline? Namely, does the low-temperature melting originate from the flatness of the potential energy surface [20] or simply because of the enormous ZPM? This query is important, because an analogous decrease of  $T_m$  has also been observed in the alkali metals such as Li [21,22] and Na [23], where NQE is insignificant. For these two elements, the  $T_m$  rises again at higher pressures. Considering the similarity of metallic hydrogen ( $H_M$ ) with the alkali metals [24], it is reasonable to expect that hydrogen should also follow a similar trend. A consequent supposition is that the potential softening could be limited, and the energy surface (ES) of  $H_M$  in this pressure range might still be rough, with noticeable energy wells and barriers. If true, this will provide profound insight into the phase stability of solid  $H_M$ , because thermally driven forces will diminish with decreasing temperature if the destabilization (or melting) of a crystal is thermally activated (TA). On the other hand, when near the ground state, the only possible dynamical forces that can destabilize a lattice are ZPM or quantum tunneling, the latter a mechanism in quantum melting that has received some attention only very recently

[25]. In this hypothetical scenario, the particle tunneling length and the height and width of the barriers on the ES are the key parameters that dictate the melting behavior.

In this article we will demonstrate that within the pressure range from 500 to 1500 GPa,  $H_M$  does fall in this regime (i.e., with limited softening in the potential) and have noticeable energy barriers. One of the consequences is a strong metastability of crystalline or glass phases at low temperatures. Furthermore, the solid ground state of dense hydrogen has also been established at the level of density functional theory (DFT) with direct numerical evidence obtained by using extensive AI-PIMD simulations.

**II. METHOD AND THEORETICAL DETAILS****A. First-principles calculations**

In our calculations, the many-body electron problem is treated with DFT, and periodic boundary conditions (PBC) are used to model the solid and/or liquid phases. AIMD simulations are carried out in a microcanonical ensemble (NVE), in which the particle number  $N$ , internal energy  $E$ , and cell volume  $V$  are conserved quantities. The classical melting is modeled using the “Z-curve” method [26], in which the internal energy is adjusted by initializing different temperatures in the system. By gradually increasing  $E$  with the cell volume being fixed, the solid phase evolves into a superheated region, and then abruptly collapses to a liquid state after reaching a critical point. The thermodynamic condition immediately after the structural collapse gives exactly the melting pressure and temperature [26]. The time step for integration of the classical motion equations is 0.5 fs. A typical AIMD simulation runs 6000 time steps, corresponding to 3 ps. Note that the structure change and melting in dense hydrogen usually take place within 1 ps in *classical* MD simulations. The final pressure and temperature are obtained by statistics over the last 2000 time steps.

In AI-PIMD simulations, the quantum motion of protons is taken into account through the path integral formalism

of quantum statistical mechanics [27–29]. When evaluating the NQE in the superheating limit, eight beads along the imaginary time line are used to approximate the Trotter decomposition of the propagators. But 32 beads are also used at a pressure of  $\sim 1.5$  TPa to check the convergence of the path integral at around 300 K. In some cases, for example *Fddd* at 100 K and  $\sim 700$  GPa, more beads are used to check the impact of bead number on the (meta)stability of the solid phases. A two-phase simulation is carried out with 32 beads, whereas the enthalpies at 50 K and  $\sim 1.5$  TPa are also calculated with 64 beads. The shortest propagator is estimated by the primitive approximation [27]. It corresponds to classical motions at 2400 K for the case with  $T = 300$  K and eight beads, and 3200 K for the case with 64 beads at 50 K, which is accurate enough for our current purpose. All AI-PIMD simulations are conducted in the *NVT* ensemble, and the superheating limit is estimated by using the *heat until melting* strategy. The melting temperature is estimated by using the NQE corrected superheating limit, together with the classical superheating degree, and the classical melting temperature difference between various  $k$ -point meshes. Alternatively, the two-phase method is also used to estimate the melting temperature. Most AI-PIMD simulations run to 5 ps, with the last 1 ps taken for thermodynamic properties statistics. In two-phase simulations, however, a longer simulation time is used, to ensure the structural equilibrium, where the averaged AI-PIMD simulation time is between 7 and 10 ps. As usual, we did not include exchange operations in AI-PIMD simulations, since protons are well separated from each other even in the liquid phase at 50 K, as [19] reported.

In both AIMD and AI-PIMD we use the same simulation cell, if without specific statement, 480H/cell for *Fddd* and liquid phase, and 432H/cell for Cs-IV phase, respectively. The forces required in the equations of motion for protons in both AIMD and AI-PIMD are calculated by density functional theory, using VASP—a code based on plane-wave methods [30]. The projector augmented-wave (PAW) pseudopotential is employed to describe the proton-electron interactions [31,32]. The Perdew-Burke-Ernzerhof (PBE) [33] parametrizations for the electron exchange-correlation energy functional are used. It is worth mentioning that previous work revealed that a semilocal exchange-correlation functional might not be enough for accurate calculation of properties of molecular phases of dense hydrogen, mainly due to the poor description of the van der Waals interactions. However, after hydrogen dissociates into an atomic phase, comparative studies showed that PBE works well in this regime [13,34–36], which is exactly the region we are interested in.

The potential energy surface is generated with various  $k$ -point sampling meshes (KPM). A case of two high symmetry special  $k$  points (2KP) is adopted to sample the Brillouin zone: one is the gamma point and the other at half along the (111) direction of an orthorhombic cell (the high-symmetry point  $R$ ); they are reweighted so as to give a best description of the total energy and pressure, in a spirit analogous to the Baldereschi mean value point [37–39]. Besides this, regular meshes with a size varied from  $2 \times 2 \times 2$  up to  $4 \times 4 \times 4$  are also used. The convergence of the  $k$  points is carefully checked, which shows that the total energy and pressure are fully converged with a  $3 \times 3 \times 3$  mesh.

Unless specifically noted, most AIMD simulations are carried out with the  $3 \times 3 \times 3$   $k$ -points mesh; whereas due to the computational cost, AI-PIMD are usually done with a mesh of  $2 \times 2 \times 2$ , and a correction of  $A = A_{2 \times 2 \times 2} + (A_{3 \times 3 \times 3} - A_{2 \times 2 \times 2})_{\text{AIMD}}$  is applied when necessary. The cutoff for the kinetic energy of the plane-wave basis is 600 eV, which is high enough for MD simulations. Increasing this energy cutoff to 800 eV does not give different results. This setting of the DFT computational parameters produces a stress tensor (as well as the pressure) with an uncertainty less than 1 GPa, which is good enough for our purpose here.

## B. Projected pair correlation function

An angularly averaged pair correlation function (PCF) is a powerful tool to detect structural changes. It is defined as

$$g(r) = \frac{V}{N^2} \sum_{i \neq j}^N \delta(r_{ij} - r), \quad (1)$$

where  $r_{ij}$  denotes the distance between particle  $i$  and  $j$ . In a homogeneous liquid,  $g(r)$  becomes the well-known radial distribution function. This function, as the prefix “angularly averaged” implies, removes all orientation dependence and the anisotropy of a solid system. The projected PCF, which we will define now, on the other hand, is an attempt to bring the underlying anisotropy back, while keep the simplicity of the mathematical operations. This function is valuable for us in discovering an exotic phase of  $H_M$  that is anisotropy but flowing like a liquid.

The projected PCF along direction  $\vec{k}$  is defined as

$$G_{\vec{k}}^-(\rho) = \frac{S}{N^2} \sum_{i \neq j}^N \delta(r_{ij}^\perp - \rho). \quad (2)$$

Here  $S$  is the projection area, and the distance between particle  $i$  and  $j$  on the projection plane is  $r_{ij}^\perp = \|(\vec{r}_i - \vec{r}_j) \cdot (1 - \vec{k}\vec{k})\|$ , where  $\|\cdot\|$  denotes taking the vector length. Obviously if the system is two dimensional and perpendicular to the projection direction, then  $G_{\vec{k}}^-(\rho)$  is identical to the angularly averaged PCF  $g(r)$  on that plane. It is worth noting that projected PCF depends on the geometry of the projected region. However, for the regular orthorhombic cell, projection along the Cartesian directions always gives well-defined results.

Specifically, if the system is a homogeneous liquid, then one can derive a simple relation between  $g(r)$  and  $G(\rho)$ . Considering a reference particle, all other particles surround it with a distribution function given by  $g(r)$ . This can be viewed as being composed by a series of spherical shells. Then the projected PCF can be obtained by the following identity (derived from particle conservation):

$$\frac{2\pi\rho\Delta\rho}{S} G(\rho) = \frac{4\pi}{V} \int_{r>\rho} r^2 g(r) \frac{\Delta S(\rho)}{4\pi r^2} dr, \quad (3)$$

where  $\Delta S(\rho)$  is the area of the infinite thin strips on the spherical shells that are perpendicular to the projection direction and have a radius of  $\rho$ . Simple geometrical analysis

gives  $\Delta S(\rho) = 4\pi r \rho \Delta \rho / \sqrt{r^2 - \rho^2}$ , thus we have

$$G(\rho) = \frac{2S}{V} \int_{r>\rho} \frac{r g(r)}{\sqrt{r^2 - \rho^2}} dr. \quad (4)$$

Projection of a series of spherical shells onto a plane is not as simple as the projection of an orthorhombic cell: the geometry factor  $S/V$  is difficult to determine here. For practical purposes we cut the shells by using a cylinder with equal height and diameter, and then project the shells within the cylinder onto its base plane. The thickness of the projected region generated in this way is about the same order of the cell dimension as our MD simulations. An instructive example for the application of projected PCF is given in the Supplemental Material (SM) [40]. Here we only note that if the system is anisotropic, then the projected PCFs along different directions will show different behavior; and if there is long-range ordering then the projected PCF will have distinct features. In contrast, the projected PCF of homogeneous liquid is independent of projection direction, with a simple feature of monotonic increasing of  $G(r)$  to the first peak and then quickly growing featureless at larger distances.

### C. Richardson extrapolation

In the primitive approximation of the path integral, the dependence of the integrated quantities such as the energy on the number of beads  $N_b$ , is scaled as [41]

$$E = E_0 + A_2 N_b^{-2} + A_4 N_b^{-4} + \dots, \quad (5)$$

when  $N_b \rightarrow \infty$ . Therefore, extrapolation of AI-PIMD results evaluated at finite  $N_b$  to the infinite one can be done using the Richardson scheme, which works well for most system when  $N_b$  is large enough [41]. The extrapolation formula is

$$E_\infty = E_2 + \frac{(N_{b1}/N_{b2})^2}{1 - (N_{b1}/N_{b2})^2} (E_2 - E_1). \quad (6)$$

We extrapolate the AI-PIMD internal energy and pressure with this formula using 32 and 64 beads, respectively. We believe these values of  $N_b$  are large enough, and they are the most accurate calculations that can be done with our currently available computational resources. Comparing the enthalpy difference calculated with 32 and 64 beads at 50 K and 1.5 TPa, we found that they are not qualitatively different. Therefore, we are confident in this setting, and believe that this extrapolation provides at least qualitatively correct results, which is enough for our current purpose.

### D. Enthalpy correction

Most of our calculations are performed at constant volumes, thus the resultant pressure is slightly different for different phases with various number of beads. In order to compare the relative stability and to align the enthalpy at the same pressure, the following correction to the enthalpy has been made:

$$H(P) = H(P_0) + \Delta P V_0 - \frac{\Delta P^2 V_0}{2B(V_0)}. \quad (7)$$

Here the pressure difference with respect to a given volume  $V_0$  is  $\Delta P = P - P_0$ . The bulk modulus is taken as 3.4 TPa,

which is a good estimate for dense hydrogen at the studied pressure range [20]. It should be pointed out that the correction is insensitive to the bulk modulus for our interested cases here, and the third term was found to be insignificant. As can be seen in Fig. 6, that will be shown below, the correction is almost linear, indicating the reliability of this approximation to the enthalpy.

### E. Potential energy surface exploration

In quantum mechanics, the motion of protons is governed by the Hamiltonian  $H = T_I + U(\mathbf{R})$  within the Born-Oppenheimer approximation, where  $T_I$  is the nuclear kinetic operator and  $U(\mathbf{R})$  is the potential energy surface felt by nuclei. One of our primary purposes in this article is to characterize the features in  $U(\mathbf{R})$ , and its role (as well as that played by  $T_I$ ) on the cold melting of dense hydrogen. In order to approach the thermodynamic limit, we employ a large enough simulation cell (480H for *Fddd* and 432H for Cs-IV phase, respectively). To explore the energy surface of such a big system directly is an insurmountable task. Fortunately, since we care about only the main characteristics of the energy surface, we can take advantage of the fact that in a classical system with conservative force fields, the probability for an equilibrated system to jump out of a potential well (and to overcome an energy barrier as well) is roughly proportional to the temperature. Using this property one can extract the desired information from classical AIMD simulations.

Figure 1 illustrates the principle and the strategy we used to assess  $U(\mathbf{R})$ . Starting from a given solid phase (point A), by gradually heating the system, the crystal will fluctuate and finally reach point B where it cannot resist the thermal disturbance anymore, consequently collapsing into other solid or liquid phases. The temperature at this point corresponds to the superheating limit (SL)  $T_{sl}$ , which can be viewed as an effective measure of the potential well depth. Similarly, immediately after collapsing into a liquid

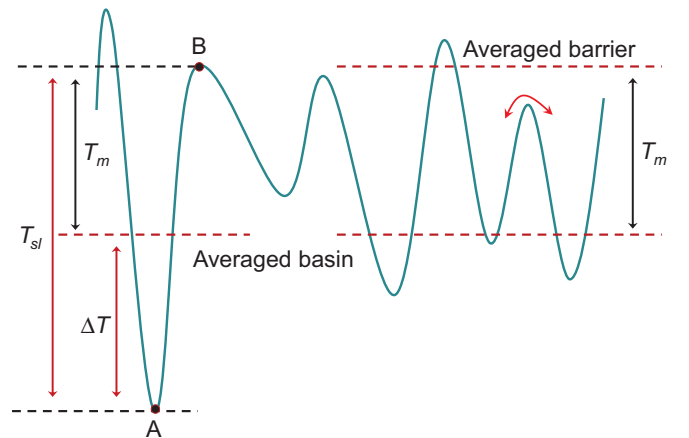


FIG. 1. (Color online) Schematic of an energy surface and the strategy of using classical kinetic energy (or equivalently the equilibrium temperature) to explore the surface's main characteristics. Note that classical  $T_m$  provides a practical estimate of the averaged barrier height, and  $T_{sl}$  gives an assessment of the well depth of the initially solid phase.

phase, the equilibrium temperature (i.e., the classical  $T_m$ ) gives the minimal classical kinetic energy that is required for the system to travel freely across all underlying barriers in the energy surface. Therefore,  $T_m$  can be taken as a measure of the averaged height of the energy barriers surrounding the initial solid phase. The difference  $\Delta T = T_{sl} - T_m$ , or the superheating degree (SD), gives a simple estimate of the static energy difference between the liquid and the initially solid phase.

The “Z-curve” method [26] just mentioned above, in which it is the internal energy rather than the temperature that is tuned, is an ideal tool for this purpose. At the point of lattice collapsing the internal energy of the solid and the liquid should be equal, i.e.,  $E_s(T_{sl}) = E_l(T_m)$ . Destruction of the crystalline structure leads to a redistribution of this energy between kinetic and potential parts, thus changing the equilibrium temperature and pressure accordingly. Though the Z method is simple to use and usually works well, it was also reported that sometimes it overestimates the  $T_m$  by up to 30% [42,43]. It is interesting to notice that almost all of these reported cases are related to a small simulation cell and heavy elements. In order to examine the performance of the Z method in dense hydrogen, we calculate the melting temperature of *Cmca-4* phase. The Z-method result is 581 K at 310 GPa, in a perfect agreement with Liu *et al.*'s two-phase method (using *NPT* ensemble) result of 580 K at 300 GPa [15]. Therefore, we conclude that it is unlikely that our method used here will have a large overestimation of the classical superheating limiting and melting temperature in dense hydrogen.

### III. RESULTS AND DISCUSSIONS

#### A. Limited potential softening

In our AIMD calculations, both Cs-IV [44] and *Fddd* phases are used as the solid candidates. *Fddd* is a low-symmetry distortion of Cs-IV and degenerate in enthalpy with the latter as the (currently proposed) least enthalpy crystalline phase [20] of  $H_M$  in the pressure range studied (see Supplemental Material for their structural connections [40]). Inclusion of *Fddd* has two purposes: (i) to improve the reliability of the computational results by coverage of a broad low-lying phase space; and (ii) because of the geometric connection between these two structures, there might be dynamic oscillations between them, which, if observed, are a precursor of quantum melting [20].

Typical Z curves calculated at  $\sim 1.5$  TPa are shown in Fig. 2. The indication is that the estimated initial well depth is about 450 K (or 39 meV), and the averaged barrier height underlying the liquid phase is  $\sim 350$  K (or 30 meV) [45]. In terms of the static energy, the initial Cs-IV or *Fddd* phase is favored by about 18 meV (in average) against transient structures in the liquid phase. This is in line with previous static lattice calculations, where an enthalpy difference of the order of ten meV/H among low-lying structures was reported [20,24]. Different resolutions in *k*-point mesh (KPM) are also examined. As can be seen from Fig. 2, this changes the energy surface moderately, especially in the case of two special *k* points (2KP) where the relative stability of solid phases has been qualitatively changed (as indicated by the negative  $\Delta T$ ).

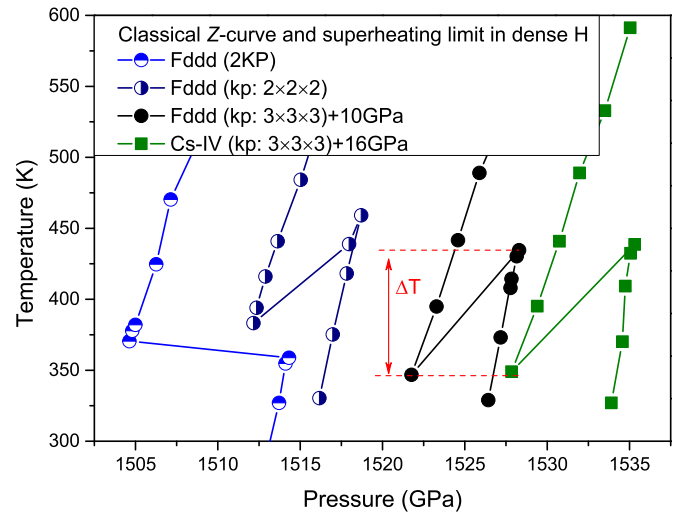


FIG. 2. (Color online) Typical Z curves in the  $P$ - $T$  plane for  $H_M$  at around 1.5 TPa calculated with AIMD simulations using the *NVE* ensemble and different *k*-point meshes.

It is necessary to point out that we did not observe any phase fluctuations. A single-way transition from Cs-IV to *Fddd* does occur in the case of 2KP, but it is not an oscillation. The same conclusion also holds in AI-PIMD simulations, in which the NQE has been included. This observation implies that the precursor of a quantum melting is difficult to achieve. It also suggests that when approaching the thermodynamic limit, *Fddd* and Cs-IV are distinct phases, and their respective basins in the phase space do not merge into a single one [20].

The convergence in our estimated energy surface shape can be inferred from Fig. 3, in which the classical  $T_m$  as a function of pressure and its variation with respect to different *k*-point meshes are plotted. It can be seen that the energy surface converges with a  $3 \times 3 \times 3$  *k*-points mesh or higher for the cell size we used. The deviation in the

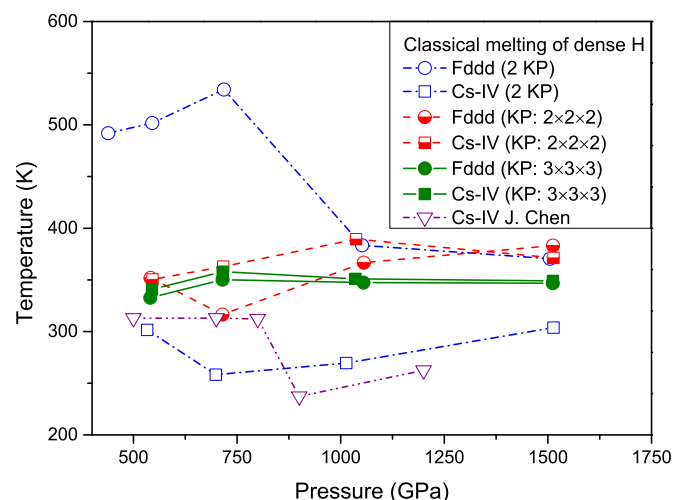


FIG. 3. (Color online) Convergence of the classical melting curve of  $H_M$  calculated with the Z-curve method using AIMD simulations in the *NVE* ensemble. Notice the large error that resulted from insufficient KPM sampling. The data of Chen are from [19].

$T_m$  of  $Fddd$  from that of Cs-IV phase, especially for those calculated with low  $k$ -points meshes, is a strong indicator that these two phases are physically distinct. By comparison, the results reported by Chen *et al.* [19], as our 2KP case here, underestimated the energy barrier by a magnitude of 50–100 K, thus underestimated the stability of the Cs-IV phase as well. When the pressure increased from 500 GPa to 1.5 TPa, our calculation shows that the density of  $H_M$  increases 56%, and the averaged interatomic distance reduced by  $\sim 0.18$  Å. This volume shrinkage, however, does not change the main characteristics of the energy surface very much. An important information conveyed by this (about which we did not have any knowledge before) is that the potential softening in  $H_M$  is limited, and the main features of energy surface (e.g., the averaged barrier height) have a very weak pressure dependence, which is corroborated by the flatness in the calculated classical  $T_m$ .

## B. Nuclear quantum effects

### 1. Assessment with perfect lattice

The above AIMD analysis revealed two important facts: (i) though  $Fddd$  and Cs-IV phases are distorted structures with each other, they respectively have independent basins, and thus are distinctly different phases; and (ii) the potential softening in  $H_M$  is limited, and reaches a flat level when above 500 GPa. With this insightful understanding one can conclude that any further descent in  $T_m$  must be because of the nuclear quantum effects. Now we turn to discuss how NQE lowers the melting temperature.

It is well known that in addition to the barriers in the potential energy surface that determine the degree of difficulty for a system to travel from one coordinate configuration into another, destabilization or melting of a lattice is also governed by a kinetic operator  $T_I$ , which generates the dynamical driving forces to overcome the energy barriers. This gives rise to the thermal noise in the classical case, and the NQE in a quantum one. The former depends only on the temperature, whereas the latter is also affected by nuclear masses and localization of the wave function, and manifests itself in ZPM and/or tunneling. From the prospect discussed above, the continuous descent of  $T_m$  beyond 500 GPa as predicted in [19] must be a consequence of NQE. There are three mechanisms by which NQE can lower the  $T_m$ : (1) quantum motion of nuclei leads to a correction term to the free energy of the solid and liquid phases (e.g., zero point enthalpy), thus changes their equality position; (2) the potential well of the solid phases is too shallow to hold the eigenstates of lattice vibrations, resulting in spontaneous delocalization of the nuclear wave function; and (3) identical particle statistics, i.e., exchanges of identical particles, further contributes to the free energy of the liquid phase, and also enhances the probability for particles to tunnel through the potential barriers [25]. Within our studied temperature range that is above 50 K, exchange in the liquid phase is negligible [19], thus in the following we do not consider case (3), and only the first two mechanisms will be investigated.

The NQE on the superheating limit can be estimated by AI-PIMD simulations [28,29]. Since this occurs at relatively high temperatures, only eight beads were used to discretize the integral path. At 1.5 TPa,  $T_{sl}$  obtained in this way is about

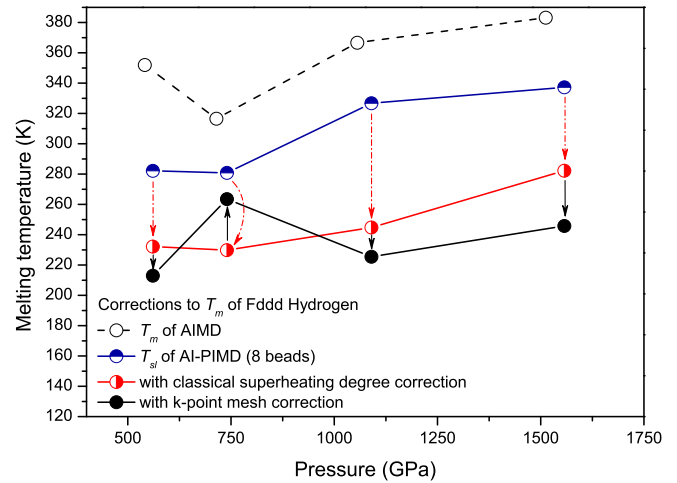


FIG. 4. (Color online) Comparison of the melting curves of  $H_M$  calculated with AIMD and AI-PIMD simulations. The latter uses eight beads to capture the NQE on the superheating limit. Corrections with respect to the classical superheating degree and  $k$ -point meshes are also plotted.

330 K. Using 32 beads slightly lowers the  $T_{sl}$  to 310 K. This small change indicates that it is adequate to use eight beads for this purpose. In contrast, the classical  $T_{sl}$  is  $\sim 450$  K. One simple and crude way to assess the NQE corrected  $T_m$  from  $T_{sl}$  is by subtracting from it the classical superheating degree  $\Delta T$ . The results obtained are shown in Fig. 4 by comparison to the classical  $T_m$  calculated with AIMD using the same DFT setting. Also shown is the further correction to account for the convergence of  $k$ -point meshes. Note that these results are below room temperature, but higher than 200 K. The high  $T_{sl}$  indicates that the NQE has limited effects to destabilize the lattice. Or to put it in other words, if the actual  $T_m$  is at ultralow temperatures as reported in [19], the solid phases should have strong metastability against melting.

An inference from Fig. 4 is that there is no spontaneous delocalization of the nuclear wave function, hence the second mechanism mentioned above is disproved. This suggests that melting of  $H_M$  in this pressure range is thermally activated, and can be described by adding a quantum correction term to the free energy functional of a classical model. To solidify this argument, one needs an additional calculation to show that the solid phases are robust against spontaneous quantum melting, especially at low temperatures where protons have long de Broglie thermal wavelength, thus long tunneling length. For this purpose we carried out direct AI-PIMD simulations of the  $Fddd$  phase at 100 K under 700 and 1000 GPa using 24 beads. The results indeed show that  $Fddd$  is at least metastable under these conditions. Using the same setting as [19] (200H/cell) and increasing the number of beads from 32 to 36, we also checked the Cs-IV phase at 1 TPa and 100 K, which confirms the (meta)stability of Cs-IV phase against spontaneous melting. Extensive calculations using 128 beads also prove the (meta)stability of solid  $H_M$  at 50 and 100 K under 700 GPa, in which due to the exceptional computation cost only 36 H/cell and 32 H/cell were used for the Cs-IV and  $Fddd$  phase, respectively. At 1.5 TPa and 50 K, long enough AI-PIMD simulations with 64 beads also confirm

that solid  $Fddd$  phase is stable. In all of these simulations, no tunneling event was observed. This finally establishes the thermally activated melting mechanism of dense hydrogen.

The above analysis suggests NQE cannot result in the continuous descent of melting temperature of  $H_M$  within the pressure range from 500 GPa to 1.5 TPa. It also implies that some other thing might occur when above 1 TPa. In order to show this and to clarify the discrepancies with Ref. [19], as well as to further consolidate the above conclusions, we turn to the direct two-phase simulations in the next subsection.

## 2. Two-phase method estimation

The computation of [19] suggested that the  $T_m$  of  $H_M$  beyond 1 TPa might be below 50 K, which is inconsistent with the above analysis. Their calculation did not answer the question of whether  $T_m$  approaches absolute zero or not, nor whether the destabilization of the solid phases is due to thermal noise or just because of NQE. On the other hand, our analysis presented above suggests strong stability of solid phases and the diminishing of driving forces at low temperatures. By contrast, in Ref. [19] the structural relaxation was reported to equilibrate very rapidly. This is inconsistent with the scenario suggested by Fig. 4 too. Considering the two-phase method in the  $NVT$  ensemble as used in Ref. [19] is prone to ambiguous results, especially at low temperatures, one might be suspicious about its conclusion [40]. In order to address these discrepancies, we repeat the two-phase AI-PIMD simulations in the  $NVT$  ensemble using 32 beads, the same as in Ref. [19]. To reduce the impact of residual stress and energy on the results, three additional strategies are employed: (i) using a large cell with a 480H/cell, rather than the 200H/cell as in Ref. [19]. This allows more flexible distortions to dissipate the stress and strain energy. (ii) Relaxing the initial two-phase coexistent configurations using AI-PIMD with the mass centers being fixed, so as to remove the residual stress and energy largely; and (iii) at the initial stage of the full AI-PIMD simulations, a small time step of 0.2 fs was used to increase the integration accuracy of the equations of motion, which is effective in reducing the unwanted nonequilibrium disturbances to the system.

The results of the two-phase simulations are surprising, though not totally unexpected. Different from Ref. [19], we find that  $H_M$  liquefies smoothly and rapidly only at temperatures higher than 250 K. At lower temperatures, the two phases are found to coexist for a long time. Even after the initial solid phase already becomes unrecognizable, the system still requires a long time to equilibrate. This observation is totally in line with the picture implied in Fig. 4: low temperature reduces the thermal driving forces, thus hinders the transformation among configurations, whereas the quantum motion of nuclei is not enough to destabilize the structure. For most of these simulations, the final equilibrated state is not the true homogeneous liquid. Rather it is an intermediate state between liquid and solid phase. On one hand, it is very similar to the liquid phase, both by visual identification and commonly used inspection tools, such as the angularly averaged PCF as shown in the inset of Fig. 5 where the calculated  $g(r)$  for three different temperatures are almost identical and show typical liquid features, as well as the

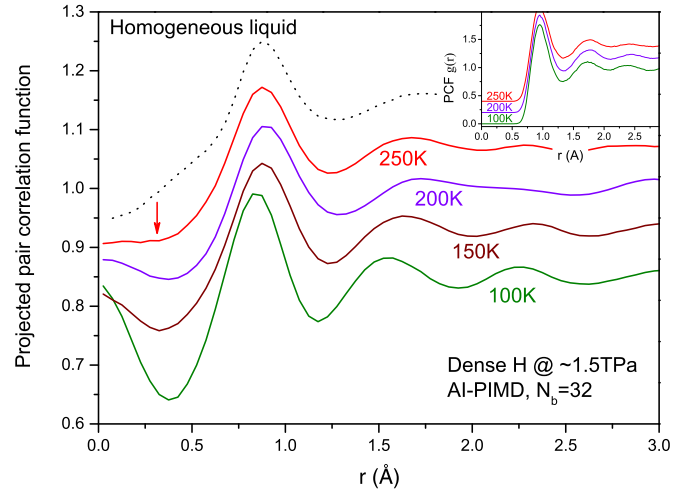


FIG. 5. (Color online) Variation of the projected PCF in  $H_M$  with temperature at a pressure of  $\sim 1.5$  TPa, after a long ( $\sim 6$  ps) two-phase equilibrating. The arrow indicates the beginning of the homogeneous liquid feature. Lines are relatively shifted for presentation.

mean square displacement (not shown). On the other hand, it has anisotropy and some long-range ordering, being analogous to a solid. Figure 5 plots the projected PCF along the  $Z$  direction, by comparison to that of the homogeneous liquid. The projected PCFs along the  $X$  and  $Y$  directions are similar to the homogeneous liquid one, thus are not shown here. The drastic difference between these projected PCFs indicates that this phase is anisotropic when below 250 K. Also note that the peaks at the null projection distance reveal that in this phase the particles prefer to align along the  $Z$  direction, a kind of long-range ordering. Therefore, we can confidently conclude that this phase is not a homogeneous liquid, and  $H_M$  does not melt at these thermodynamic conditions.

Figure 5 suggests that this exotic phase melts to the homogeneous liquid at about 250 K. As the temperature decreases, its difference from that of the true liquid becomes more striking. A similar state was also observed in *heat until melting* simulations of the  $Fddd$  phase at  $\sim 1$  TPa and 1.5 TPa (termed as phase  $D$  [40]). So why did Ref. [19] obtain a low temperature liquid state down to 50 K in their two-phase simulations? The most plausible explanation is that they mistook this exotic phase as the true liquid, since they employed the traditional angularly averaged PCF and mean squared displacement that are incapable of distinguishing these two phases. That is, failure to detect this fluidlike but nonliquid state and mistaking it as the true liquid might be the main reason that led Chen *et al.* to claim an ultralow  $T_m$ . One additional strong evidence that supports this argument is that in our two-phase simulation this exotic phase is found stable down to below 100 K. On the other hand, our two-phase simulation also reveals that the solid  $Fddd$  phase is favored at 50 K [40], thus predicting a phase boundary between them at about 75 K under  $\sim 1.5$  TPa. As Fig. 3 shows, the DFT setting of Ref. [19] underestimated the stability of the Cs-IV phase by 50–100 K. Hence it is very possible that in their calculations this phase boundary is pushed down below 50 K. As for the fast equilibrating they observed in  $H_M$ , it can be

readily explained by their uncontrolled two-phase simulation in the  $NVT$  ensemble, where artificial driving forces accelerate the relaxation process.

### C. Stability of solid phase when approaching 0 K

Our two-phase simulations suggested that the solid  $Fddd$  phase is favored against the liquid at low temperature, and it transforms into the fluidlike but anisotropic state with long-range ordering when above 75 K, the latter then melts to the homogeneous liquid state at about 250 K when at a pressure of  $\sim 1.5$  TPa. This is consistent with the estimation of  $T_m$  given in Fig. 4. We will provide another strong evidence that further supports this picture below. That is, we are going to evaluate the relative stability of the solid and liquid phases when approaching 0 K. To address this issue, usually one will resort to the principle of minimal free energy to determine which one is the favored phase. Calculation of free energy is cumbersome and computationally demanding. We thus take the advantage of the fact that the internal energy of both the harmonic and anharmonic phonons of  $H_M$  already converge to their respective zero point energy, and the difference between zero point energy and the free energy is less than  $10^{-5}$  eV/H at 50 K [40]. Please note that even though the harmonic approximation is very crude for dense hydrogen, the qualitative magnitude of its internal energy and free energy are nevertheless reliable. For this reason we can simply compare the enthalpy at 50 K to assess the relative stability of the liquid and solid phases as 0 K is approached.

The enthalpies calculated with AI-PIMD using 32 and 64 beads, and the extrapolation to infinite number of beads [41], are shown in Fig. 6 for both the liquid and solid  $Fddd$  phases, respectively. It may be seen that the solid phase is always favored over the liquid one. The enthalpy difference is about 16 meV/H in the case with 32 beads, and decreases to 14.7 meV/H when using 64 beads. The converged result obtained by Richardson extrapolation [41] is 14.3 meV/H.

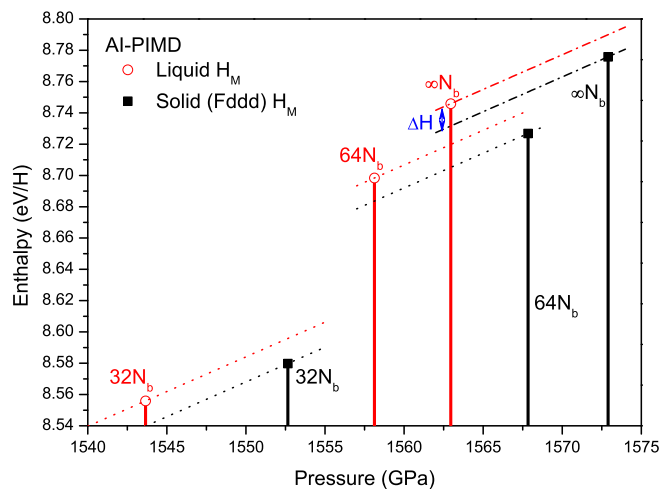


FIG. 6. (Color online) Comparison of the enthalpy of  $Fddd$  and the liquid phase of  $H_M$ , calculated using AI-PIMD at 50 K with 32 and 64 beads, respectively, and the extrapolated results to the infinite beads. Dotted and dash-dotted lines extrapolate the enthalpy to nearby pressures.

Therefore, we find that inclusion of the quantum motion of protons does not confer the liquid phase much advantage. This observation establishes direct numerical evidence at the DFT level that dense hydrogen is actually in a solid ground state when at around 1.5 TPa.

From our extensive AI-PIMD calculations for the solid phases at 50 K, it seems unlikely that there will take place a spontaneous delocalization of the nuclear wave function at lower temperatures. In the cases we have studied, the dispersion of the integral paths in solid phases is confined mainly by the potential well, rather than by the de Broglie thermal wavelength. Therefore, lowering the temperature might not enhance the tunneling probability very much. Inclusion of the identical particle exchanges is also unlikely to change the melting temperature qualitatively, since the contribution of exchanges to the free energy of the liquid phase is expected to be small (e.g., it is at a level of  $\sim 1$  K for  $^4\text{He}$  [25]), whereas the enthalpy difference between the solid and liquid phases of  $H_M$  is greater than 160 K.

## IV. CONCLUSION

In summary, by decomposing the descent of the melting temperature of  $H_M$  into two separate issues, i.e., the interaction potential softening and the dynamic driving forces from thermal noise or quantum ZPM, we presented a complete solution for the former by using AIMD simulations and the Z-curve method to evaluate the classical superheating limit and the melting curve of  $H_M$ . The second issue was also addressed by using AI-PIMD simulations, which revealed that inclusion of NQE would lower the superheating limit and melting curve accordingly. Within the pressure range from 500 GPa to 1.5 TPa, the ground state of dense hydrogen was predicted to be solid rather than the conjectured liquid. The melting/destabilizing mechanism of the crystalline phases was determined to be thermal activation. The melting temperature was estimated to be 200–250 K and has a flat variation with pressure. This provides a completely distinct picture about  $H_M$ , and defies the continuous descent of the melting temperature that was claimed previously.

## ACKNOWLEDGMENTS

This work was supported by the National Natural Science Foundation of China under Grant No.11274281, the CAEP Research Project 2012A0101001, the fund of National Key Laboratory of Shock Wave and Detonation Physics of China (under Grant No. 9140C670105130C67237), the National Science Foundation through Grant No. CHE-0910623, and also by EFree, an Energy Frontier Research Center funded by the US Department of Energy (Award No. DESC0001057 at Cornell). Computation was performed using the Extreme Science and Engineering Discovery Environment (XSEDE), which is supported by National Science Foundation Grant No. OCI-1053575, the Cornell NanoScale Facility, a member of the National Nanotechnology Infrastructure Network, which is supported by the National Science Foundation (Grant ECCS-0335765), and the resources of the Supercomputing Laboratory at King Abdullah University of Science and Technology (KAUST) in Thuwal, Saudi Arabia.

- [1] V. Diatschenko, C. W. Chu, D. H. Liebenberg, D. A. Young, M. Ross, and R. L. Mills, *Phys. Rev. B* **32**, 381 (1985).
- [2] I. F. Silvera, *Rev. Mod. Phys.* **52**, 393 (1980).
- [3] H. K. Mao and R. J. Hemley, *Rev. Mod. Phys.* **66**, 671 (1994).
- [4] A. F. Goncharov, R. J. Hemley, and H. K. Mao, *J. Chem. Phys.* **134**, 174501 (2011).
- [5] R. T. Howie, C. L. Guillaume, T. Scheler, A. F. Goncharov, and E. Gregoryanz, *Phys. Rev. Lett.* **108**, 125501 (2012).
- [6] C. S. Zha, Z. Liu, M. Ahart, R. Boehler, and R. J. Hemley, *Phys. Rev. Lett.* **110**, 217402 (2013).
- [7] F. Datchi, P. Loubeyre, and R. LeToullec, *Phys. Rev. B* **61**, 6535 (2000).
- [8] E. Gregoryanz, A. F. Goncharov, K. Matsuishi, H. K. Mao, and R. J. Hemley, *Phys. Rev. Lett.* **90**, 175701 (2003).
- [9] S. Scandolo, *Proc. Natl. Acad. Sci. USA* **100**, 3051 (2003).
- [10] S. Deemyad and I. F. Silvera, *Phys. Rev. Lett.* **100**, 155701 (2008).
- [11] M. I. Eremets and I. A. Trojan, *JETP Lett.* **89**, 174 (2009).
- [12] S. A. Bonev, E. Schwegler, T. Ogitsu, and G. Galli, *Nature (London)* **431**, 669 (2004).
- [13] M. A. Morales, C. Pierleoni, E. Schwegler, and D. M. Ceperley, *Proc. Natl. Acad. Sci. USA* **107**, 12799 (2010).
- [14] C. Attaccalite and S. Sorella, *Phys. Rev. Lett.* **100**, 114501 (2008).
- [15] H. Liu, L. Zhu, W. Cui, and Y. Ma, *J. Chem. Phys.* **137**, 074501 (2012).
- [16] N. W. Ashcroft, *J. Phys.: Condens. Matter* **12**, A129 (2000).
- [17] V. V. Kechin, *JETP Lett.* **79**, 40 (2004).
- [18] E. Babaev, A. Sudbø, and N. W. Ashcroft, *Nature (London)* **431**, 666 (2004).
- [19] J. Chen, X.-Z. Li, Q. Zhang, M. I. J. Probert, C. J. Pickard, R. J. Needs, A. Michaelides, and E. Wang, *Nat. Commun.* **4**, 2064 (2013).
- [20] H. Y. Geng, H. X. Song, J. F. Li, and Q. Wu, *J. Appl. Phys.* **111**, 063510 (2012).
- [21] C. L. Guillaume, E. Gregoryanz, O. Degtyareva, M. I. McMahon, M. Hanfland, S. Evans, M. Guthrie, S. V. Sinogeikin, and H. K. Mao, *Nat. Phys.* **7**, 211 (2011).
- [22] A. M. J. Schaeffer, W. B. Talmadge, S. R. Temple, and S. Deemyad, *Phys. Rev. Lett.* **109**, 185702 (2012).
- [23] E. Gregoryanz, O. Degtyareva, M. Somayazulu, R. J. Hemley, and H.-k. Mao, *Phys. Rev. Lett.* **94**, 185502 (2005).
- [24] J. M. McMahon, M. A. Morales, C. Pierleoni, and D. M. Ceperley, *Rev. Mod. Phys.* **84**, 1607 (2012), and references therein.
- [25] M. Boninsegni, L. Pollet, N. Prokof'ev, and B. Svistunov, *Phys. Rev. Lett.* **109**, 025302 (2012).
- [26] A. B. Belonoshko, N. V. Skorodumova, A. Rosengren, and B. Johansson, *Phys. Rev. B* **73**, 012201 (2006).
- [27] D. M. Ceperley, *Rev. Mod. Phys.* **67**, 279 (1995).
- [28] D. Marx and M. Parrinello, *J. Chem. Phys.* **104**, 4077 (1996).
- [29] H. Y. Geng, *J. Comput. Phys.* **283**, 299 (2015). In this study, only a single level sampling of the potential is employed, i.e., the standard primitive approximation.
- [30] G. Kresse and J. Furthmüller, *Phys. Rev. B* **54**, 11169 (1996).
- [31] P. E. Blöchl, *Phys. Rev. B* **50**, 17953 (1994).
- [32] G. Kresse and D. Joubert, *Phys. Rev. B* **59**, 1758 (1999).
- [33] J. P. Perdew, K. Burke, and M. Ernzerhof, *Phys. Rev. Lett.* **77**, 3865 (1996).
- [34] M. A. Morales, J. M. McMahon, C. Pierleoni, and D. M. Ceperley, *Phys. Rev. Lett.* **110**, 065702 (2013).
- [35] M. A. Morales, J. M. McMahon, C. Pierleoni, and D. M. Ceperley, *Phys. Rev. B* **87**, 184107 (2013).
- [36] M. A. Morales, C. Pierleoni, and D. M. Ceperley, *Phys. Rev. E* **81**, 021202 (2010).
- [37] B. Holst, R. Redmer, and M. P. Desjarlais, *Phys. Rev. B* **77**, 184201 (2008).
- [38] W. Lorenzen, B. Holst, and R. Redmer, *Phys. Rev. B* **82**, 195107 (2010).
- [39] A. Baldereschi, *Phys. Rev. B* **7**, 5212 (1973).
- [40] See Supplemental Material at <http://link.aps.org/supplemental/10.1103/PhysRevB.92.104103> for extended discussion.
- [41] L. Brualla, K. Sakkos, J. Boronat, and J. Casulleras, *J. Chem. Phys.* **121**, 636 (2004).
- [42] J. B. Haskins, J. A. Moriarty, and R. Q. Hood, *Phys. Rev. B* **86**, 224104 (2012).
- [43] D. Alfe, C. Cazorla, and M. J. Gillan, *J. Chem. Phys.* **135**, 024102 (2011).
- [44] K. A. Johnson and N. W. Ashcroft, *Nature (London)* **403**, 632 (2000).
- [45] The actual depth should be doubled, which is exact for a harmonic potential. But we take it as an effective measure here, hence only the kinetic energy part is used explicitly.